# Electronic transitions in the ion-molecule reaction $(Ar^+ + H_2 \leftrightarrow Ar + H_2^+) \rightarrow ArH^+ + H$

M. Baer
*Department of Theoretical Physics and Applied Mathematics, Soreq Nuclear Research Center, Yavne, Israel and Department of Chemical Physics, Weizmann Institute of Science, Rehovot, Israel*

J. A. Beswick
*Laboratoire de Photophysique Moléculaire, Université de Paris-Sud 91405 Orsay, France*
(Received 18 April 1978)

A collinear reactive study of the ion-molecule system ($Ar + H_2^+$, $Ar^+ + H_2$, $ArH^+ + H$) is presented. The main emphasis was directed towards the two reactions $Ar^+ + H_2(v = 0) \rightarrow ArH^+ + H$ and $Ar + H_2^+(v' = 2) \rightarrow ArH^+ + H$, which exhibit avoided-crossing features. It is shown that reactive transition probabilities obtained from an exact collinear treatment which incorporated a large number of vibrational states to ensure convergence are reproduced by simple reactive curve-crossing models.

## I. INTRODUCTION

The process whereby electronic transitions are induced during an atom-diatom collision has recently become the subject of many theoretical studies.[1] The ion-molecule reaction

$$(Ar^+ + H_2 \rightleftarrows Ar + H_2^+) \rightarrow ArH^+ + H \tag{1}$$

provides an example of the importance of electronic transitions in reactive systems.[2-10] In the asymptotic region of the reactants $(Ar \cdots H_2)^+$ the two lower surfaces cross along the vibrational coordinate $r$ of the two hydrogen nuclei at low energy. Therefore the adiabatic description of this region is clearly inadequate as it implies an abrupt change in the electronic structure. In the diabatic picture the two surfaces correspond asymptotically to the electronic states $Ar^+(^2P_{3/2}) + H_2(^1\Sigma_g)$ and $Ar(^1S) + H_2^+(^2\Sigma_g)$ and define the two channels on the left-hand side of reaction (1). In the asymptotic region of the products $(ArH \cdots H)^+$ the two surfaces lie far apart, the lower one leads to a stable molecule $ArH^+$ $(X\,^1\Sigma) + H$ and the upper is repulsive and corresponds to $ArH(^2\Sigma) + H^+$. It therefore seems that the diabatic picture is the best representation to describe reaction (1). However, Kuntz and Roach[11] have shown that as the ground state of $ArH^+$ dissociates into $Ar + H^+$, only the reactant state $Ar + H_2^+$ correlates with the ground state of $ArH^+$. Thus maintaining the diabatic representation and ignoring the diabatic coupling terms would imply that of the two reactions

$$Ar^+ + H_2 \rightarrow ArH^+ + H, \quad \Delta E = -1.65 \text{ eV}; \tag{2a}$$

$$Ar + H_2^+ \rightarrow ArH^+ + H, \quad \Delta E = -1.30 \text{ eV}; \tag{2b}$$

only the second is possible, while the first as well as the charge-transfer reaction

$$Ar + H_2^+ \rightarrow Ar^+ + H_2, \quad \Delta E = -0.35 \text{ eV}, \tag{2c}$$

are not allowed.

In fact experimental evidence shows that reactions (2a) (Refs. 2–6) and (2c) (Ref. 7) have large cross sections, or rate constants, indicating that considerable mixing between the diabatic electronic states should exist.

In what follows we shall show that the coupling or the mixing of the two states is indeed most important. However, it will also be shown that the mixing takes place only for large values of the translation coordinate $R$ in the entrance channel. This fact calls for a simplified model which assumes surface crossing in the reactant channel before the strong interaction region is reached so that the probability for reaction will, in fact, be the probability for reaching this region. A similar model is employed in the Langevin theory for ion-molecule reactions[12] and has also been applied for treating crossing problems of the type described above[13-20] Recently Baer presented a preliminary comparison between results obtained from an exact collinear quantum-mechanical treatment and such a model.[19] The results show good qualitative agreement, in spite of the fact that only two (vibrational) states were incorporated in the model.

In this work we present a complete report of exact and approximate calculations for the collinear model of reaction (1) using the DIM surfaces derived by Kuntz and Roach in the energy range $0.5 \leq E \leq 0.8$ eV ($E$ is the total energy of the reactants). The adiabatic surfaces, as well as an outline of the method used to obtain the best diabatic surfaces for numerical integration purposes, are given in Sec. II. Then the results of the exact calculations are reported and discussed. In Sec. IV a simplified model for this process is pre-

 

sented and, finally, in Sec. V the results are summarized.

## II. POTENTIAL ENERGY SURFACES

The potential energy surfaces used here are the DIMZO (diatomics in molecules with zero overlap) surfaces given by Kuntz and Roach.[11] Only the doublet states are considered and if spin-orbit and rotational effects are neglected, then in the collinear configuration the Hamiltonian factors into a $4\times 4$ block and two other $2\times 2$ blocks. We consider here the two lower adiabatic surfaces of this Hamiltonian and the nonadiabatic coupling terms obtained from the derivatives of the DIMZO Hamiltonian matrix $\underline{H}$ (Ref. 8):

$$\tau_x \equiv \left\langle \zeta_1 \left| \frac{\partial}{\partial x} \right| \zeta_2 \right\rangle \simeq \underline{C}_1^{+} \frac{\partial}{\partial x} \underline{C}_2 = \frac{\underline{C}_1^{+}(\partial \underline{H}/\partial x)\underline{C}_2}{(V_2 - V_1)}, \tag{3}$$

where $|\zeta_m\rangle$ is the $m$th electronic eigenfunction and $V_m$ and $C_m$ are the $m$th eigenvalue and eigenvector of $\underline{H}$, respectively, and $x$ stands for $r$ and $R$, the two nuclear coordinates. The equipotential plots of the two adiabatic surfaces $V_1$ and $V_2$ as a function of the internuclear coordinate $R_{HH}$ and $R_{ArH}$ are given in Fig. 1. It can be seen that the lower surface which leads from reagents to products is exothermic, whereas the upper one behaves like a typical inelastic surface. To get a deeper insight, two cuts along the vibrational coordinate for two different $R$ values in the entrance channel are shown in Fig. 2. The two surfaces are in general seen to be far apart except for a short $r$ interval in the vicinity of $r \sim 0.82$ Å. Also as $R$ increases the two surfaces approach each other, and in fact as $R \to \infty$ they "almost" touch. The line along $R$ which combines all the $r$ points where the two surfaces are closest to each other is called the *seam*. In Fig. 2 the vibrational nonadiabatic coupling term $\tau_r(r, R)$ is also given. It can be seen that $\tau_r(r, R)$ peaks at the seam and that the peak becomes sharper as $R$ increases. Indeed it has been shown[21] that for large $R$ values $\tau_r(r, R)$ becomes

$$\lim_{R\to\infty} \tau_r(r, R) = \tfrac{1}{2}\pi\delta(r - r_c), \tag{4}$$

where $r_c$ is the pseudo crossing point. This behavior is expected, as will be explained later. The translational coupling term $\tau_R(r, R)$ is in general much smaller than $\tau_r(r, R)$ and for large values of $R$ it becomes zero.

Although the information concerning the potentials and the coupling terms is given in the adiabatic representation the corresponding diabatic representation was found to be more convenient for performing the calculations.[22-25] The main reason is that the adiabatic Schrödinger equation contains terms which involve first derivatives of the wave function. This prevents one from using the very efficient methods of integration now available. The transformation from the adiabatic representation to the diabatic is made through a matrix $\underline{A}(r, R)$ in such a way that if $\underline{V}(r, R)$ is the diagonal adiabatic potential matrix with elements $V_1$ and $V_2$ then the corresponding diabatic potential matrix $\underline{W}(r, R)$ is given by

$$\underline{W}(r, R) \equiv \underline{W}(\gamma) = \underline{A}_\gamma^{*}(r, R)\underline{V}(r, R)\underline{A}_\gamma(r, R), \tag{5}$$

where $\underline{A}_\gamma$ is a rotation matrix with angle $\gamma$,[23]

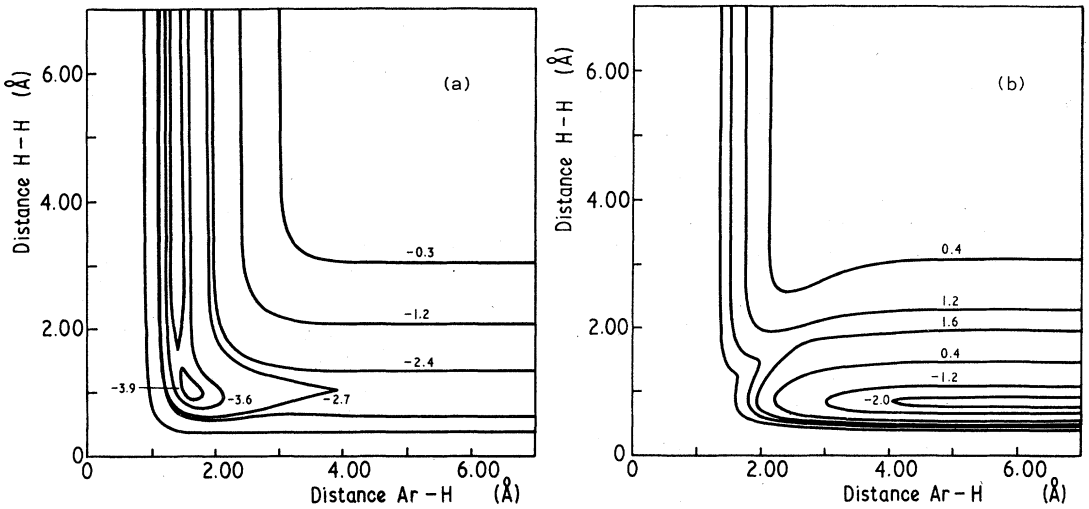


FIG. 1. Equipotential contour lines as a function of interatomic distances for the $(ArH_2)^+$ system. (a) The ground adiabatic potential surface. (b) The first excited adiabatic potential surface.

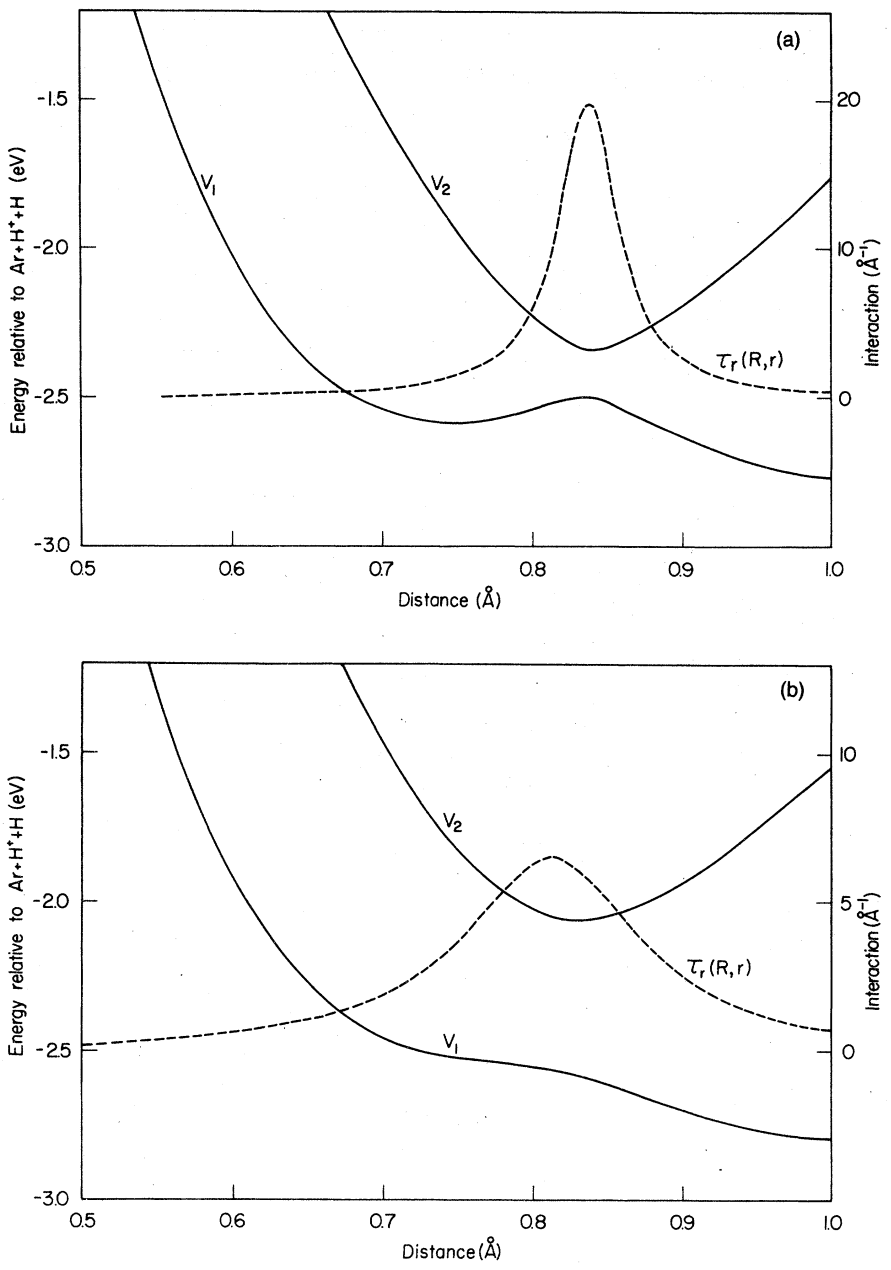


FIG. 2. Two lowest adiabatic energy levels $V_1$ and $V_2$ (——) and the corresponding vibrational adiabatic coupling term $\tau_r(r,R)$ (---) as a function of the interatomic distance $r=r_{HH}$ for a given fixed translational coordinate $R$. (a) $R=10$ a.u. (b) $R=8$ a.u.

$$\gamma=\gamma(r_0,R_0)+\int_{r_0}^{r}\tau_r(r,R_0)\,dr+\int_{R_0}^{R}\tau_R(r,R)\,dR \tag{6}$$

and the elements of $\underline{W}(\gamma)$ are

$$\begin{aligned} W_{11}(\gamma)&=V_1\cos^2\gamma+V_2\sin^2\gamma,\\ W_{22}(\gamma)&=V_1\sin^2\gamma+V_2\cos^2\gamma,\\ W_{12}(\gamma)&=W_{21}(\gamma)=\tfrac{1}{2}(V_1-V_2)\sin 2\gamma. \end{aligned} \tag{7}$$

The transformation given in (5) and (6) eliminates the first derivatives from the Schrödinger equation, which now takes the simple ordinary form

$$(\underline{T}+\underline{W})\psi=E\underline{\psi}, \tag{8}$$

where $\underline{T}$ is the usual kinetic energy operator.

With the transformation (7) now at hand, we can continue the discussion related to the asymptotic region. We shall assume that $r_0$ given in Eq. (6)

is smaller than $r_c$ [see Eq. (4)] and that

$$\gamma(r_0 < r_c, R_0 = \infty) = 0. \tag{9}$$

Then from Eq. (4), and using the fact that

$$\lim_{R\to\infty} \tau_R(r, R) = 0, \tag{10}$$

we obtain

$$\gamma = \begin{cases} 0, & r < r_c \\ \frac{1}{2}\pi, & r > r_c \end{cases} \tag{11}$$

and consequently Eq. (7) yields

$$W_{11} = \begin{cases} v_1, & r < r_c \\ v_2, & r > r_c; \end{cases}$$

$$W_{22} = \begin{cases} v_2, & r < r_c \\ v_1, & r > r_c; \end{cases} \tag{12}$$

$$W_{12} = W_{21} \equiv 0;$$

where $W_{11}$ and $W_{22}$ are the correct diatomic potentials of the $H_2$ and the $H_2^+$ molecules.

However, there is still a disadvantage in using the diabatic picture as it stands for the numerical treatment. From Eq. (7) it is seen that the diabatic coupling term $W_{12}(\gamma)$ increases with the difference between the two potential surfaces. Since in the present case one surface is attractive and the other repulsive, the difference becomes large and causes instabilities in the numerical integration. One way to avoid this problem is occasionally to perform an additional transformation similar to Eq. (5) with a constant angle $(-\gamma_0)$. This transformation yields a new potential matrix in each interval[21]

$$\underline{\overline{W}} = \underline{W}(\gamma - \gamma_0). \tag{13}$$

If $\gamma_0$ is chosen to be equal to one of the $\gamma$'s along $r$ for each $R$, namely, $\gamma_0 = \gamma(r(R), R)$, then this procedure decreases the off-diagonal term in the whole interval. This procedure defines what has been termed as *the most adiabatic-diabatic potential matrix*.[19] The reason for this terminology is that for each $R$ value there is at least one point where the diabatic and the adiabatic potentials coincide (the point where $\gamma = \gamma_0$). The line $r = r(R)$ along which the two potentials coincide is termed as the *adiabatic path in the diabatic representation*.[19]

## III. SOLUTION OF THE SCHRÖDINGER EQUATIONS

The Schrödinger equation (8) is solved by applying an integrator which was developed for this purpose by Top and Baer[25] and was successfully applied to the $(H_3)^+$ system.[21] It should be noted that although Eq. (8) is written in terms of the potential $\underline{W}(r, R)$ the exact calculations are performed with $\underline{W}(r, R) = \underline{W}(\gamma - \gamma_0)$. To do this, Eq. (8) is not solved in the original system of coordinates but in the one rotated by an angle $\gamma_0$. This change, however, forced us to propagate $\underline{\chi}(r, R)$ and not $\underline{\psi}(r, R)$ where the two are related by the transformation

$$\underline{\chi}(r, R) = \underline{A}(\gamma_0)\underline{\psi}(r, R). \tag{14}$$

Here $\underline{A}(\gamma_0)$ is the transformation matrix such that

$$\underline{\overline{W}}(r, R) = \underline{A}(\gamma_0)\underline{W}(r, R)\underline{A}^*(\gamma_0). \tag{15}$$

More details on this procedure can be found in Ref. 21.

Most of the calculations were performed with 48 states of which 18 belong to the upper surface and 30 to the lower one. Some of the states are presented as a function of the reaction coordinate in Fig. 3. The calculations were performed in the (total) energy range of 0.502–0.80 eV. Here $E = 0.502$ corresponds to the threshold for the collision of $Ar^+ + H_2(v = 0)$. The lower states in the $(Ar - H_2)^+$ asymptotic region are shown in Fig. 4. It can be seen that for the $Ar^+ + H_2$ system at most three states are open, whereas for the $Ar^+ + H_2$ only one state is open.

Figure 5 shows the total transition probabilities as a function of translational energy $T$ for the reaction

$$Ar^+ + H_2(v = 0) \rightarrow ArH^+ + H, \tag{16}$$

as well as for the charge-transfer reaction

$$Ar^+ + H_2(v = 0) \rightarrow Ar + H_2^+. \tag{17}$$

The main features are (a) a long threshold region $0 < T < 0.1$ eV, (b) large reactive transition proba-

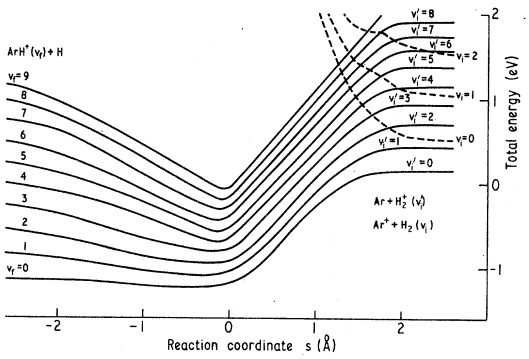


FIG. 3. Vibrational levels of the two surfaces as a function of the reaching coordinate $s$. (——) Vibrational levels of the lower surface $\overline{W}_{11}(r, R)$; (---) Vibrational levels of the upper surface $\overline{W}_{22}(r, R)$.

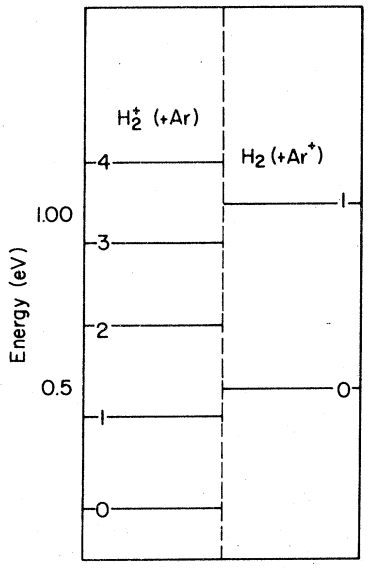


FIG. 4. Schematic picture of the asymptotic vibrational energy levels for the two diabatic potential surfaces.

bilities (~1.0) for $T > 0.1$ eV, (c) a sharp negative spike in the reactive probability function at $T = 0.11$ eV and a corresponding peak in the charge-transfer probability function, (c) low charge-transfer probabilities (< 0.1).

The transition probabilities as a function of total energy $E$ for the reactions

$$Ar + H_2^+(v' = 0, 1, 2) \rightarrow ArH^+ + H \qquad (18)$$

are presented in Fig. 6. It can be seen that in the energy range studied the transition probabilities for $v' = 0, 1$ are consistently close to unity. A long threshold region $0.0 \leq T \leq 0.1$ eV is evident for $v' = 2$, similar to that for reaction (16).

Qualitative explanations for most of the listed features can be obtained from Fig. 3. First we note that the reaction probability from these states is always close to 1 because the two lowest vibrational states of $H_2$ are below the upper surface and no potential barrier is encountered. The threshold behavior for the systems $H_2^+(v' = 2) + Ar$ and $H_2(v = 0) + Ar^+$ can be attributed to the avoided crossing related to the two states. In the pure diabatic picture reaction (16) should not happen at all and reaction (18) for $v' = 2$ should be direct with a short energy range for the threshold. However, due to the diabatic coupling terms reaction (16) becomes allowed but the long threshold region is a result of the potential barrier formed by the avoided crossing. The $Ar + H_2^+(v' = 2)$ system is first prohibited by the above avoided crossing but then becomes allowed due to the avoided crossing formed with $v' = 3$. Again the barrier that is created in this process is responsible for the long threshold region. A detailed quantitative study of this problem is presented in Sec. IV.

The sharp dip in the reaction probability function around $E = 0.11$ eV is probably due to a quasibound state which exists at the close interaction region ($s \sim 0$). From the width we can estimate its lifetime to be of the order of $10^{-12}$ sec which is three orders of magnitude larger than any vibrational period in this system. Although Fig. 3 suggests the possibility of bound states along the reaction coordinate for high vibrational levels, the pseudo potential well still seems to be too shallow to yield the spike. It is more likely that the quasibound state is the result of the formation of a complex in the turning region involving vibrational motion along and perpendicular to the reaction path.

For the sake of completeness two final vibrational distributions due to reaction (16) are presented in Fig. 7. The first is for $T = 0.099$ eV and the second for $T = 0.299$ eV. It can be seen that a strong vibrational inversion is encountered similar to those obtained in other exothermic reactions based on LEPS potentials. We shall not extend the discussion on these results because they were

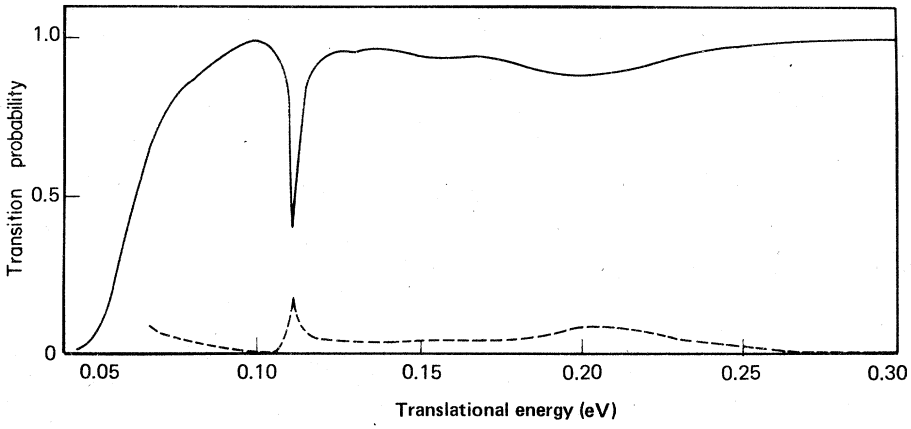


FIG. 5. Reactive and charge-transfer probabilities as a function of translational energy $T$. (——) $Ar^+ + H_2$ ($v = 0$) → $ArH^+ + H$; (----) $Ar^+ + H_2$ ($v = 0$) → $Ar + H_2^+$.

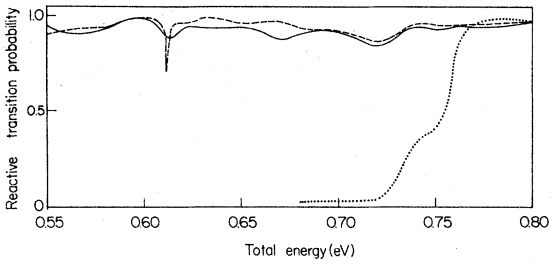


FIG. 6. Reactive transition probability as a function of total energy. (——) $Ar + H_2^+$ ($v = 0$) → $ArH^+ + H$; (---) $Ar + H_2^+$ ($v = 1$) → $ArH^+ + H$; (• • •) $Ar + H_2^+$ ($v = 2$) → $ArH^+ + H$.

not stable enough with respect to variations of certain numerical parameters which define the integration. Although the inverstion was consistently observed, the results tend to change. Thus we found for instance in a different calculation that the vibrational distribution for $T = 0.099$ eV was peaking at $v = 6$ instead of at $v = 5$.

## IV. CURVE-CROSSING MODEL FOR THE $Ar^+ + H_2(v=0)$ AND $Ar + H_2^+(v'=2)$ REACTIONS

In this section a simplified model of curve crossing for reaction (16) and the reaction

$$Ar + H_2^+(v' = 2) \rightarrow ArH^+ H \tag{18'}$$

is presented. As already mentioned the region where electronic nonadiabatic transitions occur is in the reactants channel and is well separated from the strong interaction region ($s \sim 0$). If we assume that the strong interaction region as well as the products channel have only a minor effect on the reactive transition probability, then the probability for a reaction to occur is equal to the probability for the reactants to pass the electronic interaction region. This model was already tested before,[19] i.e., two curves were included in the model and applied to reaction (16), and it was found that such a simplified treatment would reproduce the threshold behavior of this reaction. Now the model has been extended: more states are included, improved coupling terms are employed, and reaction (18′) is studied as well.

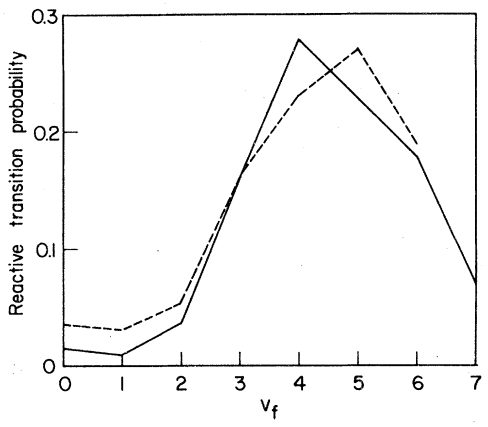


FIG. 7. Vibrational distribution of products. Results for the reaction: $Ar^+ + H_2$ ($v = 0$) → $ArH^+(v_+) + H$; (---) translational energy $T = 0.099$ eV; (——) translational energy $T = 0.299$ eV.

### A. The model

The Schrödinger equation for the general diabatic two-surface case is written

$$[T_n + \underline{\overline{W}}(R, r) - E]\underline{\chi}(R, r) = 0, \tag{19}$$

where $\overline{W}(R, r)$ given in Eq. (13) is the modified diabatic $2 \times 2$ potential matrix, $E$ is the total energy, and $T_n$ takes the form

$$T_n = -\hbar^2 \left( \frac{1}{2\mu} \frac{\partial^2}{\partial R^2} + \frac{1}{2m} \frac{\partial^2}{\partial r^2} \right). \tag{20}$$

Here $\mu$ and $m$ are the reduced masses

$$\mu = (m_{Ar} m_{H_2})/(m_{Ar} + m_{H_2}); \quad m = m_H m_H / m_{H_2}. \tag{21}$$

Expanding $\chi_i(R, r)$; $i = 1, 2$ in terms of a basis set $\eta_{ni}(R, r)$; $i = 1, 2$; $n = 0, 1, 2, \ldots$, i.e.,

$$\chi_i(R, r) = \sum_{n=1}^{\infty} \eta_{ni}(R) \phi_{ni}(R, r), \tag{22}$$

where $\phi_{ni}(R, r)$ are the solutions of the equation

$$\left( -\frac{\hbar^2}{2m} \frac{\partial^2}{\partial r^2} + \overline{W}_{ii}(R, r) - \epsilon_{ni}(R) \right) \phi_{ni}(R, r) = 0. \tag{23}$$

One obtains, assuming that the $\phi_{ni}(R, r)$ are only weakly dependent on $R$, the set of coupled equations

$$\left( -\frac{\hbar^2}{2\mu} \frac{\partial^2}{\partial R^2} + \epsilon_{n1}(R) - E \right) \psi_{n1} + \sum_{n'} \langle \phi_{n1} | \overline{W}_{12} | \phi_{n2} \rangle \psi_{n'2} = 0, \tag{24}$$

$$\left( -\frac{\hbar^2}{2\mu} \frac{\partial^2}{\partial R^2} + \epsilon_{n2}(R) - E \right) \psi_{n2} + \sum_{n'} \langle \phi_{n2} | \overline{W}_{12} | \phi_{n'1} \rangle \psi_{n'1} = 0.$$

The validity of the assumption concerning the dependence of $\phi_{ni}(R, r)$ on $R$ is only justified outside the strong-interaction region ($s \sim 0$). Conse-

quently this model can be applied only when the electronic nonadiabatic transitions occur in a region which is far enough from that region as in the $(Ar+H_2)^+$ system.

Let us now introduce a matrix $\underline{w}$ such that

$$\begin{aligned} &\underline{w}_{ll}(R)=\epsilon_{ni}\,; \quad i=1,2, \quad n=0,1,2,\ldots\,; \\ &\underline{w}_{kl}=\langle\phi_{ni}\,|\,W_{12}\,|\,\phi_{n'i'}\rangle(1-\delta_{ii'})\,; \end{aligned} \tag{25}$$

and a wave function $\underline{\zeta}$ such that

$$\zeta_l=\eta_{ni}\,; \quad i=1,2\,, \quad n=0,1,2,\ldots\,. \tag{26}$$

Then Eq. (24) becomes

$$\left(-\frac{\hbar^2}{2\mu}\frac{\partial^2}{\partial R^2}+\underline{w}-E\right)\zeta=0 \tag{27}$$

which is now the ordinary set of Schrödinger equations usually encountered in curve-crossing problems.

Equation (27) is also solved like an ordinary inelastic curve-crossing problem, however, with one difference which is related to the "reactive" nature of some of the curves. Open states are not only expected on the right-hand side of the electronic interaction (the ordinary asymptotic region) but also on its left-hand side.

Thus since $R$ is assumed to vary in the range $-\infty\leq R\leq\infty$, for $R\to\infty$ we have for the open states the ordinary asymptotic conditions: i.e.,

$$\xi_{ll_0}=\delta_{ll_0}\exp(-ik_{l_0}R)/\sqrt{k_{l_0}}+R_{ll_0}\exp(ik_lR)/\sqrt{k_l} \tag{28}$$

and for $R\to-\infty$

$$\xi_{ll_0}=T_{ll_0}\exp(-ik_l'R)/\sqrt{k_l'}\,. \tag{29}$$

Here

$$\begin{aligned} &k_l=\{(2\mu/\hbar^2)[E-w_{ll}(R\to\infty)]\}^{1/2}, \\ &k_l'=\{(2\mu/\hbar^2)[E-w_{ll}(R\to-\infty)]\}^{1/2}, \end{aligned} \tag{30}$$

and $R_{ll_0}$ and $T_{ll_0}$ are related to the transition probabilities

$$P^R_{ll_0}=|R_{ll_0}|^2, \quad P^T_{ll_0}=|T_{ll_0}|^2; \tag{31}$$

where $P^T_{ll_0}$ is the inelastic transition probability and $P^R_{ll_0}$ is the reactive transition probability.

### B. Results

In what follows $\underline{w}$ is a matrix either of order $2\times2$ or $3\times3$. The first diagonal term always stands for the state $v=0$ of the $A^+ + H_2$ system (surface 2) and the other diagonal elements stand for the vibrational states $v'=2,3$ of the $Ar+H_2^+$ system (surface 1). Thus

$$\begin{aligned} &w_{11}=\epsilon_{02}; \\ &w_{ll}=\epsilon_{n1}; \quad n=2,3, \quad l=2,3\,. \end{aligned}$$

$w_{12}$ and $w_{13}$ are the electronic coupling terms which are assumed to be different from zero, $w_{23}$, which is the coupling term between two states that belong to the same manifold, is usually small and is therefore ignored.

To perform the numerical calculations all the matrix elements were presented in analytical forms

$$\begin{aligned} &w_{11}=0.5+0.19\exp[-4.5(R-4.4)], \\ &w_{12}=0.68\tanh[2.11(R-3.5)], \\ &w_{33}=w_{22}+0.24, \\ &w_{12}=w_{13}=14.52\exp[-1.15R], \\ &w_{23}=0. \end{aligned} \tag{32}$$

The numerical values of the various parameters were determined in such a way to make a best fit with the vibrational states (see Fig. 3) and the coupling terms that were extracted from the exact calculations. All the energies are given in eV and the distances in Å. The curves representing the diagonal elements (diabatic potentials) and the corresponding adiabatic potentials obtained after diagonalizing $\underline{w}$ are plotted in Fig. 8.

In order to solve the coupled diabatic equations we use the same method as in the exact treatment. The interval of integration is divided into subintervals. In each subinterval a transformation $\underline{Q}$ is defined such that

$$\underline{D}=\underline{Q}^*\underline{W}\underline{Q} \tag{33}$$

is diagonal in the *middle point*. In this way $N$ solutions $\eta_i$, $i=1,2,\ldots,N$ are formed, where $\eta_i$ is the solution in the $i$th subinterval of the coupled Schrödinger equations:

$$\left(-\frac{\hbar^2}{2\mu}\frac{\partial^2}{\partial R^2}+\underline{D}_i-E\right)\underline{\eta}_i=0\,. \tag{34}$$

The $\underline{\eta}_i$ eigenvectors are related to the original $\underline{\zeta}_i$ eigenvectors by

$$\underline{\eta}_i=\underline{Q}_i\underline{\zeta}_i \tag{35}$$

and the transformation from $\underline{\eta}_i(R)$ to $\underline{\eta}_{i+1}(R)$ at the matching point $R=R_i$ is given as

$$\eta_{i+1}(R=R_i)=\underline{Q}_{i+1}\underline{Q}_i^*\,\underline{\eta}_i\,(R=R_i)\,. \tag{36}$$

The results of the model calculations are presented in Figs. 9(a) and 9(b) where they are compared with the exact results for reactions (16) and (18′). For both cases we applied the two- and three-state models. For reaction (16) the two-state model yields results which qualitatively fit the exact results (see also Ref. 19), however, the fit is improved by adding the third state and the two curves almost overlap along the entire energy range studied, except for the spike at $T=0.11$

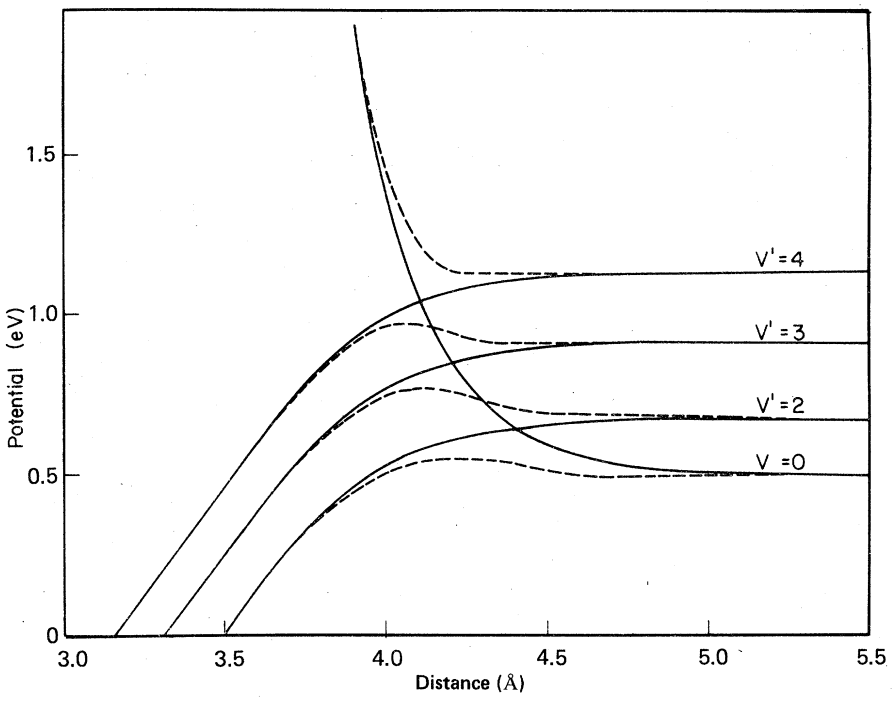


FIG. 8. Diabatic and the adiabatic curves as a function of the translational coordinate $R$. The diabatic curves are obtained from Eq. (32) and the adiabatic ones are the eigenvalues of the $w$ matrix. (——) Diabatic curves; (---) Adiabatic curves.

eV. For reaction (18′) the two-state model did not yield any reactive transition probabilities due to the avoided crossing between $v=0$ of the $Ar^+ + H_2$ system and $v'=2$ of the $Ar + H_2^+$ system. Adding the third state improved the situation dramatically (due to the avoided crossing of $v=0$ and $v'=3$ of the $Ar + H_2^+$ system) although the fit with the exact results is not as good as in the previous case.

## V. SUMMARY

In this work we presented the results of the exact and model calculations two-surface collinear ($Ar + H_2^+$, $Ar^+ + H_2$, $ArH^+ + H$) reactive system. The exact calculations were performed by a method which was previously developed and applied to the ($H_2 + H^+$, $H_2^+ + H$) reactive system. The essence of the method is the reduction of an $n$-sur-

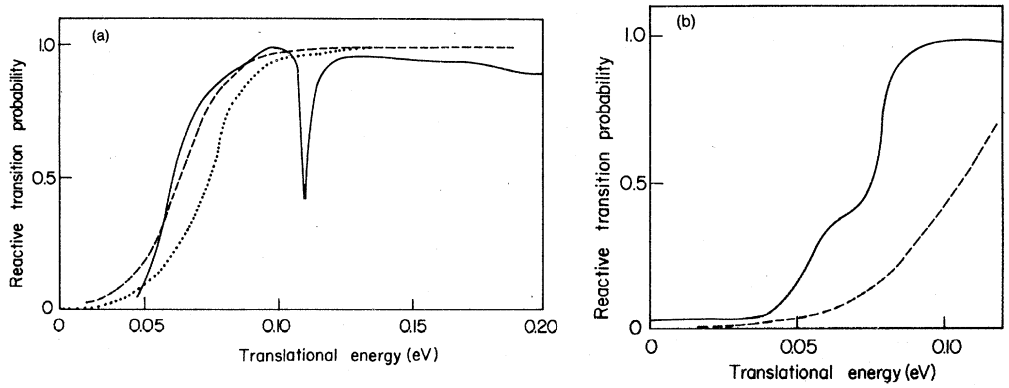


FIG. 9. Reactive transition probabilities. A comparison between exact results and model calculation results for the reactions: (a) $Ar^+ + H_2$ ($v=0$) → $ArH^+ + H$; (——) Exact results; (···) two state approximation; (---) three state approximation; (b) $Ar + H_2^+$ ($v'=2$) → $ArH^+ + H$; (——) exact results; (---) three state approximation.

face problem ($n > 2$) given in the diabatic framework to a two-surface problem. This procedure is rigorous with minimal loss of information. It was applied to the $H_3^+$ system, where the DIM method yields three surfaces, and to the present case, where the DIM yields four surfaces. The exact results were obtained by incorporating 40–50 vibrational states to ensure convergence.

The model employs diabatic reactive curves (instead of surfaces), which are the vibrational states of the original systems given as a function of the reaction coordinate, and the diabatic coupling both extracted from the exact program. Both the diabatic curves and the coupling terms were fitted to known functions and then used in the model calculation.

The emphasis in this study was on the evolution of the reactive process through the electronic nonadiabatic region which couples the two surfaces. It was found that the exact reactive transition probability function for the reaction

$$Ar^+ + H_2(v=0) \rightarrow ArH^+ + H$$

was reproduced by the model whereas the fit for the reaction

$$Ar + H_2^+(v'=2) \rightarrow ArH^+ + H$$

was less satisfactory but still reasonably close.

These results have important implications for future treatments of ion-molecule interactions in three dimensions. If the electronic nonadiabatic coupling region is well separated from the close distance interaction region (around $s = 0$) one may assume the existence of one interaction channel and treat the reactive process as an inelastic one. The only change will be the imposition of different boundary conditions on the close distance side. The fact that the results due to the model are so reliable gives hope that in the future the main effort in such studies will be devoted to the preparation of the diabatic curves (the corresponding vibrotational states) and the diabatic coupling terms and the amount of work needed for solving the scattering process will be negligibly small.

## ACKNOWLEDGMENTS

One of us (J.A.B.) is indebted to the Chemical Physics Department, The Weizmann Institute of Science, for their kind hospitality during the completion of this work. This work was supported by the U. S.-Israel Binational Science Foundation.

[1]M. S. Child, in *Atom-Molecule Collisions: a Guide for Experimentalists*, edited by R. B. Bernstein (Plenum, New York, to be published), Chap. 7.
[2]An extensive list of references is given in E. A. McDaniel, V. Cermak, A. Dalgarno, E. E. Ferguson, and L. Friedman, *Ion-Molecule Reactions* (Wiley-Interscience, New York, 1970).
[3]R. D. Smith, D. L. Smith, and J. H. Futrell, Int. J. Mass Spectrom. Ion Phys. 19, 395 (1976).
[4]N. G. Adams, D. K. Bohme, D. H. Dunkin, and F. C. Fehsenfeld, J. Chem. Phys. 52, 1951 (1970).
[5]R. K. Ryan and I. G. Graham, J. Chem. Phys. 59, 4206 (1973).
[6]M. T. Bowers and D. D. Elleman, J. Chem. Phys. 51, 4606 (1969).
[7]P. M. Hierl, V. Pacak, and Z. Herman, J. Chem. Phys. 67, 2678 (1977).
[8]S. Chapman and R. K. Preston, J. Chem. Phys. 60, 650 (1974).
[9]J. M. Yuan and D. A. Micha, J. Chem. Phys. 69, 1032 (1976).
[10]M. Baer and J. A. Beswick, Chem. Phys. Lett. 51, 360 (1977).
[11]P. J. Kuntz and A. C. Roach, J. Chem. Soc. Faraday Trans. II 68, 259 (1972).
[12]P. Langevin, Ann. Chem. Phys. 5, 245 (1905).
[13]V. I. Osherov, Zh. Eksp. Teor. Fiz. 49, 1157 (1965) [Sov. Phys. JETP 22, 804 (1966)].
[14]J. R. Laing, J. M. Yuan, I. H. Zimmerman, P. L. Devries, and T. F. George, J. Chem. Phys. 66, 2801 (1977).
[15]M. S. Child, *Molecular Collision Theory* (Academic, New York, 1974), pp. 224–234.
[16]E. Bauer, E. R. Fisher, and G. R. Gilmore, J. Chem. Phys. 51, 4173 (1969).
[17]E. E. Nikitin and S. Ya Umanski, Discuss. Faraday Soc. 53, 7 (1972).
[18]E. A. Gislason, J. Chem. Phys. 57, 3396 (1972).
[19]M. Baer, Mol. Phys. 35, 1637 (1978).
[20]M. Baer and M. S. Child, Mol. Phys. (to be published).
[21]Z. H. Top and M. Baer, Chem. Phys. 25, 1 (1977).
[22]F. T. Smith, Phys. Rev. 179, 111 (1969).
[23]M. Baer, Chem. Phys. Lett. 35, 112 (1975).
[24]M. Baer, Chem. Phys. 15, 49 (1976).
[25]Z. H. Top and M. Baer, J. Chem. Phys. 66, 1363 (1977).